


Cite this: *J. Mater. Chem. A*, 2023, 11, 9152

# Oil-paper-umbrella-inspired passive radiative cooling using recycled packaging foam†

Yang Liu,<sup>a</sup> Xiaojie Liu,<sup>a</sup> Fangqi Chen,<sup>a</sup> Yanpei Tian,<sup>ab</sup> Andrew Caratenuto<sup>a</sup> and Yi Zheng <sup>\*ac</sup>

Passive daytime radiative cooling (PDRC) is a promising energy-saving cooling method to cool objects without energy consumption. Although numerous PDRC materials and structures have been proposed to achieve sub-ambient temperatures, the technique faces unprecedented challenges brought on by complicated and expensive fabrication. Herein, inspired by traditional Chinese oil-paper umbrellas, we develop a self-cleaning and self-cooling oil-foam composite (OFC) made of recycled polystyrene foam and tung oil to simultaneously achieve efficient passive radiative cooling and enhanced thermal dissipation of objects. The OFCs show high solar reflectance (0.90) and high mid-infrared thermal emittance (0.89) during the atmospheric transparent window, contributing to a sub-ambient temperature drop of  $\sim 5.4$  °C and cooling power of  $86 \text{ W m}^{-2}$  under direct solar irradiance. Additionally, the worldwide market of recycled packaging plastics can provide low-cost raw materials, further eliminating the release of plastics into the environment. The OFC offers an energy-efficient, cost-effective and environmentally friendly candidate for building cooling applications and provides a value-added path for plastic recycling.

Received 13th February 2023  
Accepted 27th March 2023

DOI: 10.1039/d3ta00823a

rsc.li/materials-a

## 1 Introduction

Traditional cooling technologies consume around 13% of the global energy and produce large amounts of CO<sub>2</sub> emissions, which results in global warming, environmental pollution, and urban heat island effects.<sup>1,2</sup> Passive daytime radiative cooling (PDRC) is a promising future technology for building cooling and renewable energy harvesting, which can realize sub-ambient cooling performance under direct sunlight by simultaneously reflecting sunlight (0.3–2.5 μm) and emitting infrared thermal radiation to the cold outer space ( $\sim 3 \text{ K}$ )<sup>3</sup> through the mid-infrared (MIR) atmospheric transparent window (8–13 μm).<sup>4–9</sup> Recently, researchers have successfully designed numerous PDRC materials and structures with both high solar reflectance  $R_{\text{solar}}$  and high infrared thermal emissivity  $\epsilon_{\text{IR}}$  through the atmospheric window, such as photonic structures,<sup>10–14</sup> metamaterials,<sup>15–17</sup> nanoparticles,<sup>10,18–22</sup> porous structures,<sup>23–26</sup> and bio-inspired materials.<sup>27–29</sup> Although these PDRC structures have good radiative cooling performance, their designs and approaches are either complicated or expensive,

which makes them unsuitable for widespread field applications in infrastructure.

Due to the exceptional performance and low cost of polymeric materials, the global consumption of plastics continues to rise, and is expected to reach up to 417 million tons per year by 2030.<sup>30,31</sup> Polystyrene (PS), one of the most used thermoplastic polymers, is widely used in the field of building, packaging, and electronics due to its excellent processability and low dielectric properties.<sup>32</sup> However, millions of tons of PS waste are produced and discarded into the environment every year, which has resulted in a serious ecological problem. Therefore, opportunities for recycling PS have great significance and economic benefits. For example, wasted PS plastic has been studied for various recycling applications in the field of building, ceramics and electrical equipment. Here, to further enrich its recycling value, used expanded polystyrene (EPS) foam will be repurposed into PDRC materials in this research, which can also significantly decrease the cost of the PDRC materials and fabrication.

An oil-paper umbrella is a traditional umbrella used in China, which has the function of blocking rain and sunlight. Tung oil, the “oil” mentioned in the oil-paper umbrella, is a drying oil obtained by pressing the seed from the nut of the tung tree, which has been widely used to protect umbrellas, wooden furniture and buildings from getting wet, discoloration and fungal decay for over thousands of years in China.<sup>33</sup> Tung oil mainly contains unsaturated fatty acids of alpha-eleostearic acid, linoleic acid, and oleic acid,<sup>34</sup> all of which can impart

<sup>a</sup>Department of Mechanical and Industrial Engineering, Northeastern University, Boston, MA 02115, USA. E-mail: y.zheng@northeastern.edu

<sup>b</sup>Material Science Engineering, Physical Science Engineering Division, King Abdullah University of Science and Technology (KAUST), Thuwal, Saudi Arabia

<sup>c</sup>Department of Chemical Engineering, Northeastern University, Boston, MA 02115, USA

† Electronic supplementary information (ESI) available. See DOI: <https://doi.org/10.1039/d3ta00823a>

excellent water, mold, and discoloration resistances to tung oil.<sup>35</sup> The highly unsaturated conjugated system of tung oil can contribute to good performances in terms of the polymerization, mechanical characteristics and thermal stability. When tung oil is evenly sprayed on the surface of paper, it will be oxidized by oxygen and then polymerized to form a protective oil film over the paper surface, which can effectively prevent paper wetting.<sup>36</sup> Despite its many advantages mentioned above, tung oil has not been utilized in passive radiative cooling until now. Here, inspired by the traditional Chinese oil-paper umbrella, we take advantage of tung oil and recycled EPS foam to fabricate low-cost and eco-friendly passive radiative cooling materials.

In this work, we report a simple and scalable method to transform the recycled EPS foam into a self-cooling material with self-cleaning ability. Inspired by the traditional Chinese oil-paper umbrella, in which the tung oil is used to protect the paper from getting wet, we fabricate a highly solar-reflective and infrared-emissive oil-foam composite (OFC) made of recycled EPS foam and tung oil that makes the OFC waterproof, to achieve efficient daytime radiative cooling in real-world applications (Fig. 1). Due to the efficient scattering effects of the OFC's micro/nanopores, the OFC exhibits a particularly high solar reflectance of 90%. Meanwhile, the existence of tung oil not only connects the dispersed foam particles tightly together, but also protects the OFC from water wetting and dust contamination in outdoor applications. More importantly, the covered tung oil layer can significantly reinforce its mid-infrared thermal emittance ( $\epsilon_{\text{IR}} = 0.89$ ) during the atmospheric transparent window. Consequently, the OFCs exhibit an average sub-ambient temperature drop of  $\sim 5.4$  °C and cooling power of  $86 \text{ W m}^{-2}$  under direct solar irradiance, which is much better than the cooling performance of the original EPS foam board. In addition, the tung oil-like yellowish color of the OFC will achieve thermal regulation and aesthetical demands simultaneously. These advantages of the functional self-cooling

and self-cleaning composites will shed light on an alternative recycled-plastic-based radiative cooling material and provide a promising path for eco-friendly applications, especially for less developed areas.

## 2 Experimental section

### 2.1 Materials

The recycled EPS foam waste was obtained from Dell Inc. HOPE'S 100% pure tung oil was obtained from Amazon.

### 2.2 Fabrication of the OFCs

First, the EPS foam board (6 g) was rinsed with DI water, cut into small pieces, and then beaten into foam pulp using a high-speed blender for 20 min (Vitamix E310). Assisted by the vacuum filtration, the dispersed PS foam particles were hand-pressed into a foam sheet with a diameter of 90 mm and a thickness of 3 mm in a glass Petri dish. Next, the tung oil (6 g) was evenly brushed on top of the foam sheet, and placed in an oven (60 °C) for 48 h. The oil-foam sheet was then bleached with  $\text{H}_2\text{O}_2$  (30% solution) at 20 °C for 24 hours followed by subsequent washing in DI water. The bleaching effect of  $\text{H}_2\text{O}_2$  on the color and spectral reflectance of the OFC is shown in Fig. S1 and S2,<sup>†</sup> respectively. Finally, the sample was placed in an oven (60 °C) for 24 h again.

### 2.3 Fabrication of the outdoor radiative cooling experimental setup

All materials were placed inside a 100-Quart modified cooler box with excellent thermal insulation (Fig. 5a), where 25 mm thick EPS foam boards with a thermal conductivity of  $0.027 \text{ W m}^{-1} \text{ K}^{-1}$  were utilized as the insulation chamber wall. Here, two OFC samples (90 mm in diameter and 3 mm in thickness) and a wood sheet (90 mm in diameter and 0.6 mm in thickness) were placed in three separate chambers, respectively (inset of Fig. 5a). T-type

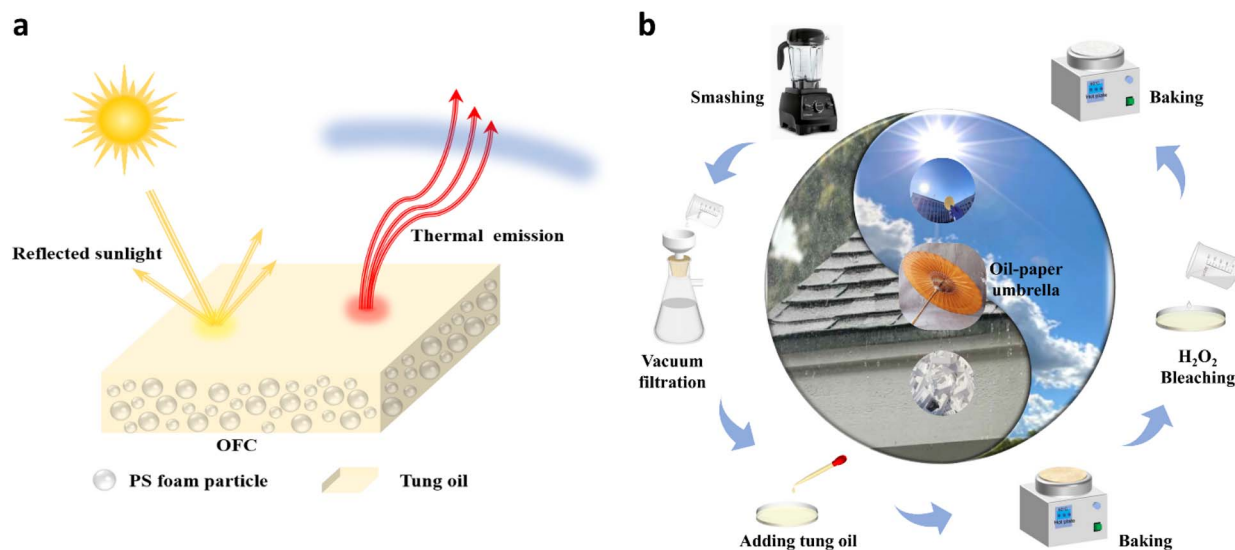


Fig. 1 Schematic illustration of the proposed approach. (a) Radiative cooling mechanism of the OFC. (b) Fabrication process inspired by a traditional Chinese oil-paper umbrella.

thermocouples were adhered to the back of samples (OFC samples and wood sheet) to measure their real-time temperatures, and these thermocouples are connected to a National Instruments (NI) PXI-6289 multifunction I/O module. The top surface of the OFC sample in Chamber 1 faced the clear sky without any windshield. For Chambers 2 and 3, the top surfaces of the OFC sample and wood sheet were covered with a 20  $\mu\text{m}$  thick low-density polyethylene (LDPE) film with a 10 mm air gap.

## 2.4 Morphology characterization

Surface morphologies of OFC samples and PS foam particle micro/nanostructures after mechanical smashing were examined by using a scanning electron microscope (SEM, S5200, Hitachi Company) at an acceleration voltage of 3 kV, respectively.

## 2.5 Optical characterization

The reflectance spectra (0.3–2.5  $\mu\text{m}$ ) were measured using a Jasco V770 spectrophotometer. The reflectance spectra (2.5–20  $\mu\text{m}$ ) were measured using a Jasco FTIR 6600. Angular-dependent reflectance spectra were measured using wedges with different angles at the sample port of these two integrating spheres.

## 2.6 Thermal conductivity measurement

Thermal conductivities of OFCs were measured by using the isotropic module of a TPS 2500s.

## 2.7 Calculation of solar reflectance and thermal emittance of OFCs

The overall hemispherical solar reflectance of the OFCs is defined and calculated as<sup>37</sup>

$$R_{\text{solar}}(\lambda, \theta, \phi) = \frac{\int_{0.3\mu\text{m}}^{2.5\mu\text{m}} I_{\text{solar}}(\lambda, \theta, \phi) R(\lambda, \theta, \phi) d\lambda}{\int_{0.3\mu\text{m}}^{2.5\mu\text{m}} I_{\text{solar}}(\lambda, \theta, \phi) d\lambda}, \quad (1)$$

where  $\lambda$  is the wavelength,  $\theta$  is the polar angle, and  $\phi$  is the azimuthal angle.  $I_{\text{solar}}(\lambda)$  is the ASTM G173 global solar intensity, and  $R(\lambda, \theta, \phi)$  is the spectral directional reflectance.

The overall hemispherical thermal emissivity of the OFCs is defined and calculated as<sup>37</sup>

$$\epsilon_{\text{IR}}(\lambda, \theta, \phi) = \frac{\int_{8\mu\text{m}}^{13\mu\text{m}} I_{\text{BB}}(\lambda, \theta, \phi) [1 - R(\lambda, \theta, \phi)] d\lambda}{\int_{8\mu\text{m}}^{13\mu\text{m}} I_{\text{BB}}(\lambda, \theta, \phi) d\lambda}, \quad (2)$$

where the wavelength range (8–13  $\mu\text{m}$ ) represents the mid-infrared (MIR) atmospheric transparent window.  $I_{\text{BB}}(\lambda)$  means the spectral intensity emitted by the blackbody.

# 3 Results and discussion

## 3.1 Preparation and characterization of multifunctional OFCs

The original EPS foam board consists of small polystyrene beads that are derived from styrene *via* a polymerization process (Fig. 2a and b).<sup>38</sup> The OFCs are fabricated by mechanically pulverizing foam particles followed by spreading tung oil evenly to form a self-cleaning and self-cooling surface (Fig. 1b and 2d). Due to the effect of tung oil, the as-prepared OFC sample shows a tung oil-like yellowish color under sunlight when observed by the naked eye, enriching the aesthetic demands of PRDC materials. The irregular-shaped PS microparticles (Fig. S3†) make up the main structure of the OFC (Fig. 2e and S4†) and are bound together by tung oil. The randomly arranged PS particles covered with tung oil can efficiently scatter sunlight from visible to near-infrared wavelengths and emit thermal radiation into the cold outer space through the atmospheric transparency window (Fig. 1a). Not only does the tung oil integrate the

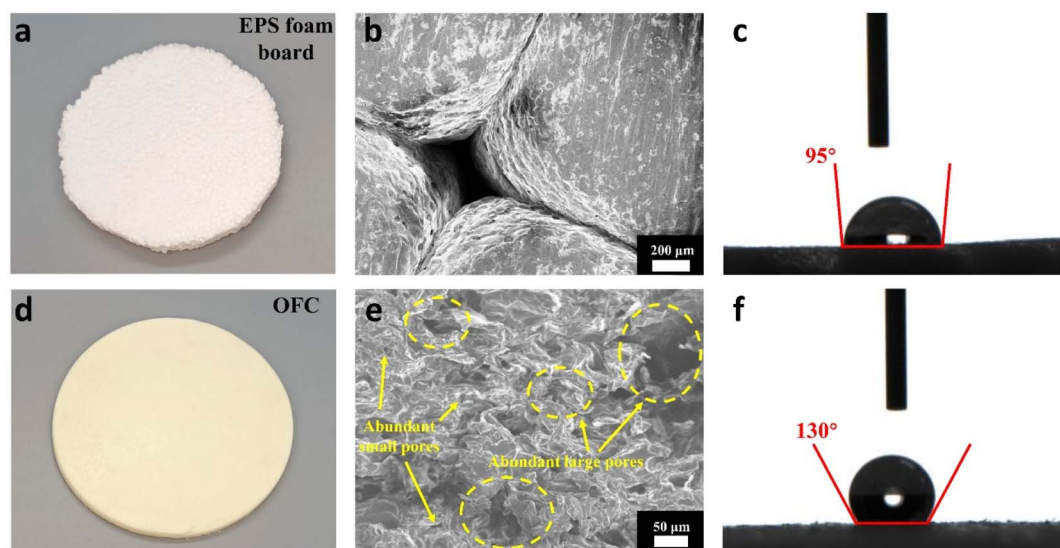


Fig. 2 Comparison of EPS and the OFC. (a and d) Optical images, (b and e) microscope images, and (c, f) water contact angle images of the as-prepared 90 mm-diameter PS foam board (10 mm in thickness) and OFC (3 mm in thickness), respectively.

network of OFC with micro/nanostructures supported by irregular-shaped PS microparticles, but it also significantly improves the hydrophobicity of the PS foam, enhancing its contact angle from  $95^\circ$  to  $130^\circ$  (Fig. 2c, f and S5<sup>†</sup>). This waterproof feature of tung oil plays a major role in the formation of the self-cleaning surface of the OFCs and aids outdoor applications. Interestingly,  $R_{\text{solar}}$  of the OFC is enhanced from 0.88 to 0.90 (Fig. 3a) after the aforementioned fabrication steps, compared with the original EPS foam board. The comparison of spectral reflectance between the OFC sample and tung-oil paper is shown in Fig. S6.<sup>†</sup> This result could be attributed to the decreased size of PS foam particles (Fig. S3<sup>†</sup>) due to machine crushing that enhances the sunlight scattering of the OFC. Compared with the regular distribution of large-size polystyrene beads with an average size of  $2000\ \mu\text{m}$  (Fig. 2c), the irregular-shaped PS microparticles form a rough surface with micro/nanopores, which can reinforce the sunlight scattering of the OFC (Fig. 2e and S4<sup>†</sup>). The combination of high solar reflectance  $R_{\text{solar}}$  and infrared emissivity  $\epsilon_{\text{IR}}$  of the OFC ensures its sub-ambient cooling effects under direct sunlight (Fig. 1a).

Since the incident angles of outdoor sunlight change over time, the angle-independent property is vital to the outdoor cooling performance of PDRC structures. Although both  $R_{\text{solar}}$  and  $\epsilon_{\text{IR}}$  of the OFCs show a little decrease with the increase in the incident angle ( $0^\circ \leq \theta \leq 60^\circ$ ), the average  $R_{\text{solar}}$  and  $\epsilon_{\text{IR}}$  are around 0.9, as shown in Fig. 3b and c, respectively. This is attributed to its rough surface with micro/nanopores made by the irregular-shaped and randomly arranged PS foam particles. The unique structure of the OFC enables a high radiative cooling performance regardless of the solar incidence angle, which is crucial for real-life applications.

Besides the optical response of the PDRC structure, its thermal conductivity should be also taken into account in terms of the thermal dissipation of radiative cooling materials. This is because sub-ambient radiative cooling requires more transport to the underlying space in real applications. The thermal conductivity of the OFC is  $0.092\ \text{W m}^{-1}\ \text{K}^{-1}$ , which is 240% higher than that of the original EPS foam board ( $0.027\ \text{W m}^{-1}\ \text{K}^{-1}$ ), and also better than that of cellulose- and organic-based materials in previously reported work about radiative cooling

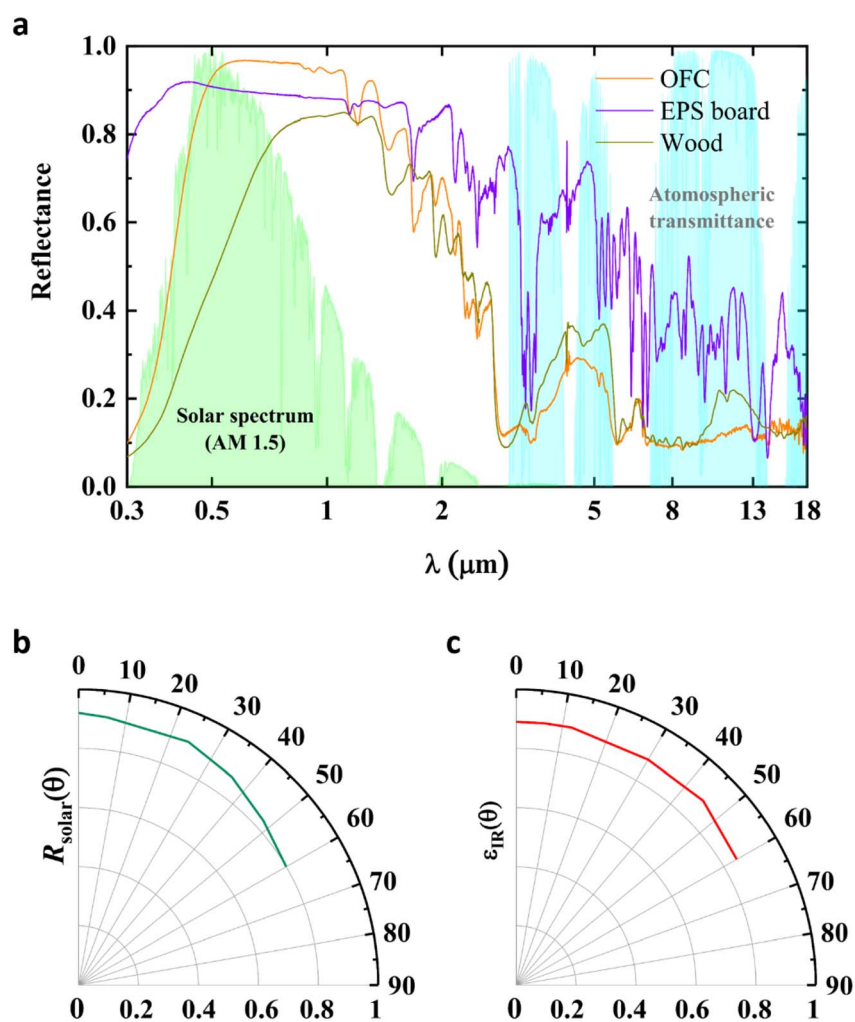


Fig. 3 Optical characterization of the OFC. (a) Hemispherical spectral reflectance of the OFC sample, EPS foam board and wood sheet plotted against the normalized AM 1.5 spectrum (ASTM G173) and the atmospheric window, respectively. (b) Angular solar reflectance and (c) angular infrared emittance of the OFC sample over wide angles of incidence.

materials.<sup>39,40</sup> The improved thermal conductivity of the OFC is due to the mechanical smashing process, which creates irregular-shaped PS foam particles and further increases the contact area with one another. Additionally, the embedded tung oil squeezes the air out of the OFC, further enhancing the OFC's inner heat transport due to higher thermal conductivity of tung oil (about  $0.167 \text{ W m}^{-1} \text{ K}^{-1}$ ) than that of air (about  $0.024 \text{ W m}^{-1} \text{ K}^{-1}$ ).<sup>41</sup> During use, the relatively high thermal conductivity of the OFC will accelerate the thermal dissipation of the underlying space in real-life situations.

### 3.2 Radiative cooling mechanism of OFCs

Tung oil (Fig. 4a) consists of alpha-eleostearic acid (82.0%), linoleic acid ([https://en.wikipedia.org/wiki/Linoleic\\_acid](https://en.wikipedia.org/wiki/Linoleic_acid)) (8.5%) palmitic acid (5.5%) and oleic acid (4.0%), and has its own intrinsic optical properties contributing to PDRC applications. The Fourier transform infrared (FTIR) transmission spectra elucidate that the OFC (PS foam particles covered with tung oil) exhibits strong emission bands at  $1050\text{--}1250 \text{ cm}^{-1}$ , which are assigned to the stretching of C–O (Fig. 4b)<sup>7,42</sup> of the four acid components of tung oil mentioned above. Therefore, compared with the EPS foam board, the presence of tung oil can greatly improve its infrared emissivity from 0.65 to 0.89 within the atmospheric transparent window. On the other hand, the negligible extinction coefficient of polystyrene from  $0.38$  to  $2.5 \mu\text{m}$  (covering the entire solar wavelength range) makes PS foam a great reflector of solar irradiance.<sup>43</sup> Furthermore, the micro/nanoporous structure of the OFCs can strongly scatter incident light at solar wavelengths ( $0.3\text{--}2.5 \mu\text{m}$ ), resulting in high reflectance of solar irradiation ( $R_{\text{solar}} = 0.90$ ). Numerous PS foam particles with different sizes act as the skeleton of the OFC, and tung oil between foam particle interfaces interconnects these particles as an adhesive to further enhance the mechanical strength. The pores among the PS particle-based structure can trap tung oil to reduce the top

surface roughness of the OFC, producing a self-cleaning functionality.

### 3.3 Daytime radiative cooling performance of the OFCs

The sub-ambient cooling performance of the OFCs during daytime (September 24, 2022) has been demonstrated on a building roof at Northeastern University, Boston, MA ( $42.36^\circ \text{ N}$ ,  $71.06^\circ \text{ W}$ ). Fig. 5a and S7† show the setup of the outdoor radiative cooling experiment with three chambers. The insets of Fig. 5a schematically illustrate the structure inside the chamber. The steady-state temperature of the OFC was measured in Chamber 1. Meanwhile, to block convective heat transfer from air, the temperature of the same OFC sample was measured in Chamber 2 with an LDPE cover, which has average transmissivities of 0.9 and 0.89 for mid-infrared and solar radiation wavelengths, respectively. A wood sheet in Chamber 3 worked as a control group to demonstrate the cooling ability of the OFCs. A weather station was used to monitor the wind speed, solar intensity, and relative humidity during the experiment period (Fig. 5a). The average solar intensity during the experimental period is  $\sim 552 \text{ W m}^{-2}$  (Fig. 5b) and the average wind speed was  $\sim 6.0 \text{ km h}^{-1}$  (Fig. 5c). The OFC in Chamber 1 without an LDPE covering can achieve an average sub-ambient temperature drop of  $\sim 5.4^\circ \text{ C}$  (Fig. 5d) and average cooling power of  $86 \text{ W m}^{-2}$  under direct solar irradiance (Fig. 5f). The radiative cooling power of the OFC is calculated by using the equation  $Q_{\text{cooling}} = h(T_{\text{Air}} - T_{\text{OFC}})$ ,<sup>11,12</sup> where the comprehensive heat transfer coefficient  $h$  is determined by using the empirical equation  $h = 2.8 + 3.0V_{\text{wind}}$ .<sup>44</sup> Since the LDPE with a solar transmissivity of around 0.9 at mid-infrared wavelengths will reflect parts of the thermal emission of the OFC and the air in the chamber, resulting in the heating of the inside of the OFC sample, the temperature of the OFC in Chamber 2 is higher than that in Chamber 1. Besides, under LDPE windshields, the average temperature of the wood sheet in Chamber 3 as

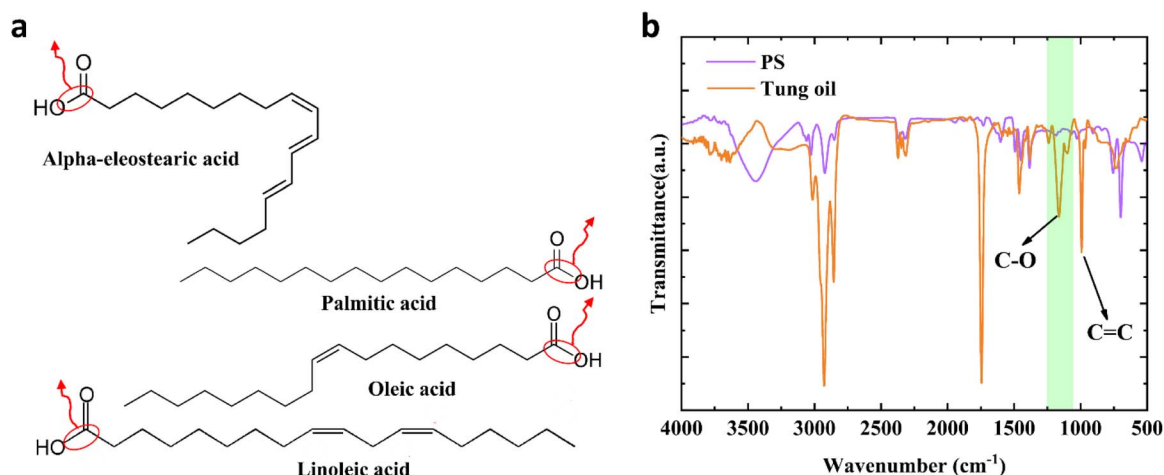


Fig. 4 Radiative cooling mechanism of OFCs. (a) Schematic showing the molecular structures of alpha-eleostearic acid, linoleic acid, palmitic acid, and oleic acid (the main components of tung oil), and the thermal emissions (red arrows) due to the molecular vibrations of C–O bands in the MIR region. (b) FTIR transmittance spectrum of the main components of tung oil presenting C–O absorption bands corresponding to the atmospheric transparent window.

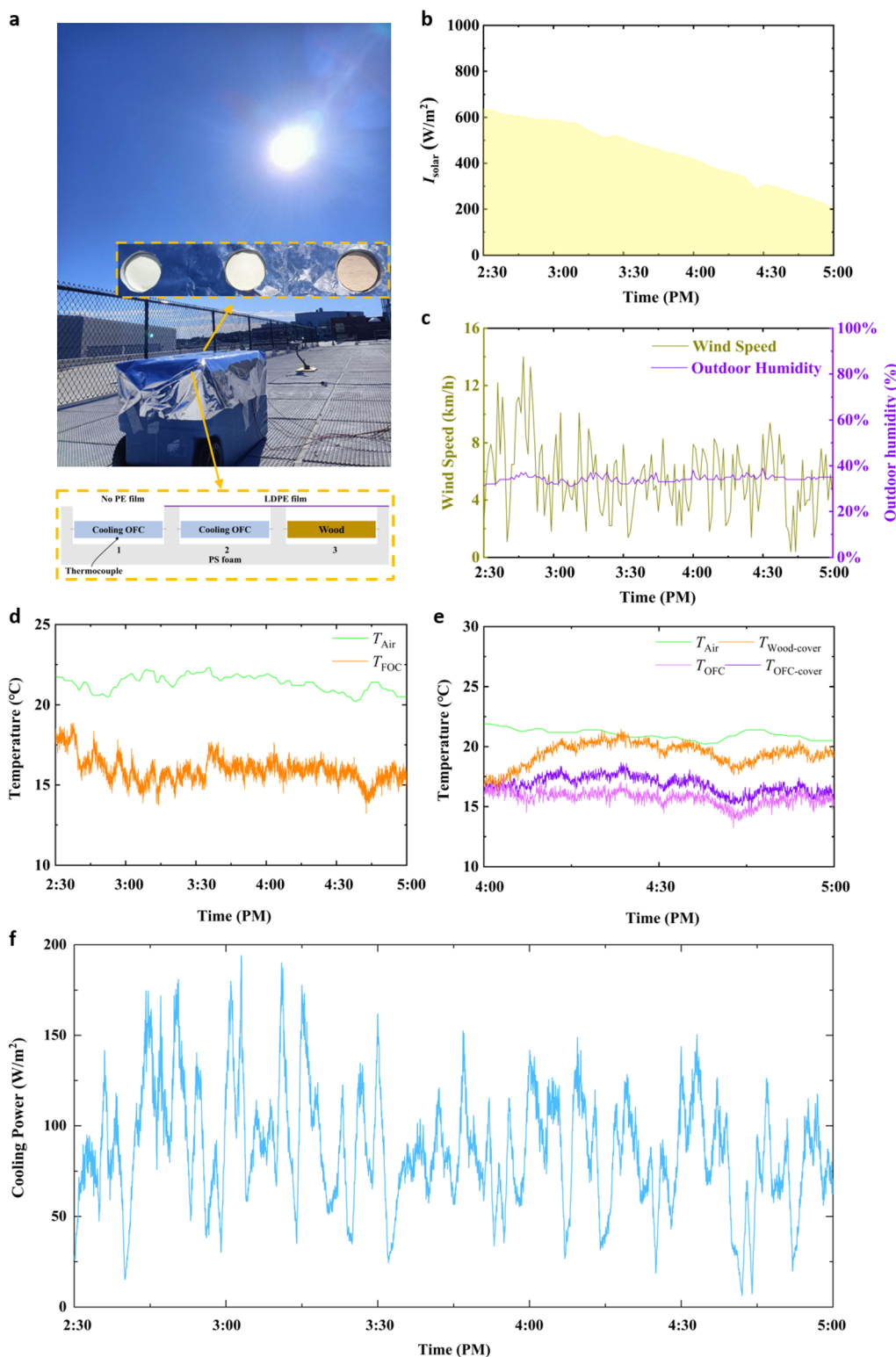


Fig. 5 Outdoor radiative cooling experiment of OFCs. (a) Photograph of the experimental apparatus for real-time measurement of passive radiative cooling performance on September 24, 2022 (Boston, MA, USA). (b) Solar intensity variations, (c) wind speed and relative humidity during the experimental period. (d) Temperature response of ambient air and the OFC sample without an LDPE cover. (e) Temperature response of ambient air, wood, and the OFC sample with an LDPE cover. (f) The radiative cooling power of the OFC calculated by using the equation  $Q_{\text{cooling}} = h(T_{\text{Air}} - T_{\text{OFC}})$ , where the comprehensive heat transfer coefficient  $h$  is determined by using the empirical equation  $h = 2.8 + 3.0V_{\text{wind}}$ .

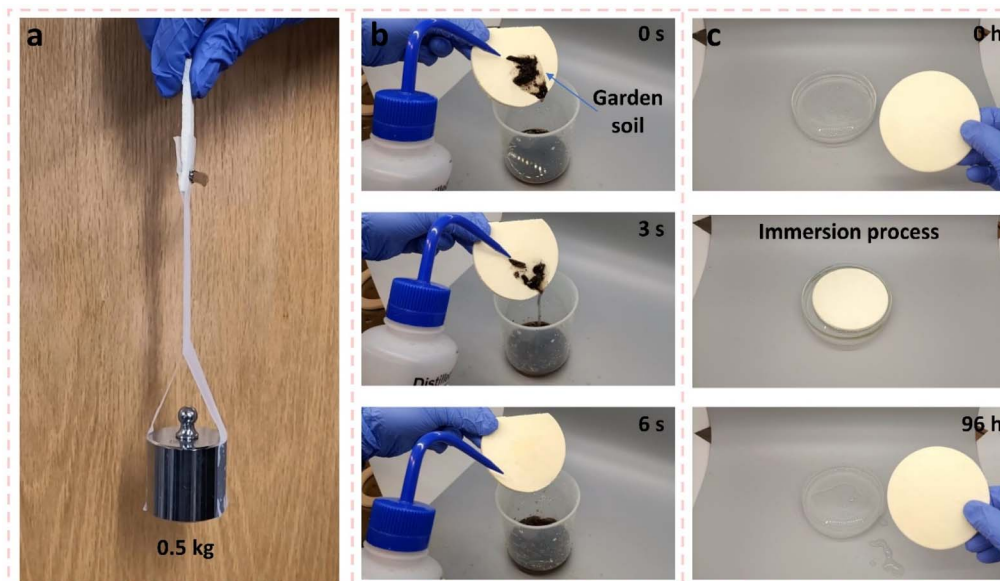


Fig. 6 Surface stability of OFCs. (a) Mechanical strength tests of the OFC. A free-standing OFC sheet (70 mm  $\times$  15 mm  $\times$  3 mm) can support a balance weight (0.5 kg). (b) Self-cleaning properties of OFCs when stained with wet garden soil. (c) Water immersion tests. OFCs are immersed in DI water in a vessel.

a control group is about 4 °C higher than that of the OFC in Chamber 2 (Fig. 5e). These temperature differences during the outdoor experiment illustrate the advantageous cooling capability of the OFCs.

### 3.4 Surface stability of OFCs

The mechanical properties of the PDRC materials are critical to various real-world applications. The OFCs are mechanically robust because of the adhesion forces of tung oil between the interfaces of the PS foam particles. Fig. 6a shows that a free-standing OFC sheet (70 mm  $\times$  15 mm  $\times$  3 mm) can easily support a weight of 0.5 kg, indicating that OFCs are suitable for engineering applications. Meanwhile, a qualified PDRC product should be resistant to environmental factors such as dust contamination, temperature and humidity changes, and exposure to rain. As such, they must maintain their optical properties and thermal performance after experiencing these conditions.<sup>18</sup> Here, we tested the anti-fouling properties of the OFCs in a simulated environment. The wet garden soil was employed to attempt to contaminate the OFC. The OFC cannot be dyed by the soil on its surface and is easily washed away without any pollution because of its excellent self-cleaning ability arising from the hydrophobic tung oil film (Fig. 6b and Video S1†). A 96 hour water immersion test exemplifies the excellent waterproof properties of the OFC vital for outdoor utilization (Fig. 6c). Besides, the weathering durability of the OFCs is demonstrated by three-month outdoor exposure with a little change observed in the spectral solar reflectance and mid-infrared thermal emittance during the atmospheric transparent window (Fig. S8†). These tests demonstrate good surface stability of the OFCs, which also experimentally confirms the value-added role of the recycled PS foam in the field of passive radiative cooling.

## 4 Conclusions

In conclusion, we have demonstrated self-cleaning and self-cooling oil-foam composites made from recycled PS foam particles. Inspired by traditional Chinese oil-paper umbrellas with the integration of tung oil, we illustrate the suitability of this material for sub-ambient daytime radiative cooling applications. The OFC has a high reflectance at solar wavelengths due to the efficient backscattering of the surface with micro/nanopores, brought on by the randomly distributed and irregularly shaped PS foam particles. Meanwhile, it also has high thermal emittance within the atmospheric transparency window because of the specific molecular bond vibrations of the covering tung oil layer. Furthermore, the addition of tung oil significantly increases the thermal conductivity of the OFCs, which can improve heat transfer from the underlying space to the top surface of the OFC. The outdoor experiment demonstrates the excellent sub-ambient cooling performance of the OFC with a sub-ambient temperature drop of  $\sim 5.4$  °C and cooling power of  $86 \text{ W m}^{-2}$  under direct solar irradiance. Moreover, the OFC possesses a self-cleaning and robust surface based on the effects of tung oil, which is a great benefit for prolonging its cooling performance in outdoor environments. In addition, the tung oil-like yellowish color of the OFC will achieve thermal regulation and aesthetical demands simultaneously. These multifunctional OFCs may inspire more radiative cooling composites purely from recycling waste plastics towards an energy-saving and sustainable society.

## Author contributions

Yang Liu: conceptualization, data analysis, writing – original draft, experimentation design. Xiaojie Liu: conceptualization,

data analysis. Fangqi Chen: sample preparation, experimental measurement. Yanpei Tian: experimentation design. Andrew Caratenuto: sample preparation, experimental measurement. Yi Zheng: supervision, resources, writing – review & editing.

## Conflicts of interest

There are no conflicts to declare.

## Acknowledgements

This project was supported by the National Science Foundation through grant number CBET-1941743 and PHY-1748958.

## Notes and references

- 1 *Cooling-Fuels & Technology*, <https://www.iea.org/fuels-and-technologies/cooling>.
- 2 K. C. S. Ly, X. Liu, X. Song, C. Xiao, P. Wang, H. Zhou and T. Fan, *Adv. Funct. Mater.*, 2022, **32**, 2203789.
- 3 D. Fixsen, *Astrophys. J.*, 2009, **707**, 916.
- 4 D. Zhao, A. Aili, Y. Zhai, S. Xu, G. Tan, X. Yin and R. Yang, *Appl. Phys. Rev.*, 2019, **6**, 021306.
- 5 S. Fan and W. Li, *Nat. Photonics*, 2022, **16**, 182–190.
- 6 X. Sun, Y. Sun, Z. Zhou, M. A. Alam and P. Bermel, *Nanophotonics*, 2017, **6**, 997–1015.
- 7 X. Yu, J. Chan and C. Chen, *Nano Energy*, 2021, **88**, 106259.
- 8 S.-Y. Heo, G. J. Lee and Y. M. Song, *J. Mater. Chem. C*, 2022, **10**, 9915–9937.
- 9 J. Liu, Y. Zhang, S. Li, C. Valenzuela, S. Shi, C. Jiang, S. Wu, L. Ye, L. Wang and Z. Zhou, *Chem. Eng. J.*, 2022, 139739.
- 10 A. P. Raman, M. A. Anoma, L. Zhu, E. Rephaeli and S. Fan, *Nature*, 2014, **515**, 540–544.
- 11 Y. Liu, M. Antezza and Y. Zheng, *Mater. Today Phys.*, 2022, **27**, 100828.
- 12 Y. Liu, Y. Tian, X. Liu, F. Chen, A. Caratenuto and Y. Zheng, *Appl. Phys. Lett.*, 2022, **120**, 171704.
- 13 D. Chae, M. Kim, P.-H. Jung, S. Son, J. Seo, Y. Liu, B. J. Lee and H. Lee, *ACS Appl. Mater. Interfaces*, 2020, **12**, 8073–8081.
- 14 H. Ma, K. Yao, S. Dou, M. Xiao, M. Dai, L. Wang, H. Zhao, J. Zhao, Y. Li and Y. Zhan, *Sol. Energy Mater. Sol. Cells*, 2020, **212**, 110584.
- 15 Y. Tian, X. Liu, Z. Wang, J. Li, Y. Mu, S. Zhou, F. Chen, M. L. Minus, G. Xiao and Y. Zheng, *Nano Energy*, 2022, **96**, 107085.
- 16 S.-Y. Heo, G. J. Lee, D. H. Kim, Y. J. Kim, S. Ishii, M. S. Kim, T. J. Seok, B. J. Lee, H. Lee and Y. M. Song, *Sci. Adv.*, 2020, **6**, eabb1906.
- 17 S. Gamage, E. S. Kang, C. Åkerlind, S. Sardar, J. Edberg, H. Kariis, T. Ederth, M. Berggren and M. P. Jonsson, *J. Mater. Chem. C*, 2020, **8**, 11687–11694.
- 18 Y. Tian, H. Shao, X. Liu, F. Chen, Y. Li, C. Tang and Y. Zheng, *ACS Appl. Mater. Interfaces*, 2021, **13**, 22521–22530.
- 19 X. Li, J. Peoples, P. Yao and X. Ruan, *ACS Appl. Mater. Interfaces*, 2021, **13**, 21733–21739.
- 20 X. Li, J. Peoples, Z. Huang, Z. Zhao, J. Qiu and X. Ruan, *Cell Rep. Phys. Sci.*, 2020, **1**, 100221.
- 21 X. Xue, M. Qiu, Y. Li, Q. Zhang, S. Li, Z. Yang, C. Feng, W. Zhang, J. G. Dai and D. Lei, *Adv. Mater.*, 2020, **32**, 1906751.
- 22 C.-H. Wang, M.-X. Liu and Z.-Y. Jiang, *Appl. Phys. Lett.*, 2022, **121**, 202204.
- 23 T. Li, Y. Zhai, S. He, W. Gan, Z. Wei, M. Heidarinejad, D. Dalgo, R. Mi, X. Zhao and J. Song, *Science*, 2019, **364**, 760–763.
- 24 D. Li, X. Liu, W. Li, Z. Lin, B. Zhu, Z. Li, J. Li, B. Li, S. Fan and J. Xie, *Nat. Nanotechnol.*, 2021, **16**, 153–158.
- 25 A. Leroy, B. Bhatia, C. C. Kelsall, A. Castillejo-Cuberos, M. Di Capua H, L. Zhao, L. Zhang, A. Guzman and E. Wang, *Sci. Adv.*, 2019, **5**, eaat9480.
- 26 M. Chen, D. Pang and H. Yan, *J. Mater. Chem. C*, 2022, **10**, 8329–8338.
- 27 N. N. Shi, C.-C. Tsai, F. Camino, G. D. Bernard, N. Yu and R. Wehner, *Science*, 2015, **349**, 298–301.
- 28 S. Jeong, C. Y. Tso, Y. M. Wong, C. Y. Chao and B. Huang, *Sol. Energy Mater. Sol. Cells*, 2020, **206**, 110296.
- 29 J. Lee, Y. Jung, M. Lee, J. S. Hwang, J. Guo, W. Shin, J. Min, K. R. Pyun, H. Lee and Y. Lee, *Nanoscale Horiz.*, 2022, **7**, 1054–1064.
- 30 Z. O. Schyngs and M. P. Shaver, *Macromol. Rapid Commun.*, 2021, **42**, 2000415.
- 31 J. Di, B. K. Reck, A. Miatto and T. E. Graedel, *Resour. Conserv. Recycl.*, 2021, **167**, 105440.
- 32 S. Wang, B. Wang, X. Zhang, L. Wang, W. Fan, H. Li, C. Bian and X. Jing, *Appl. Surf. Sci.*, 2021, **570**, 151157.
- 33 N. Thanamongkollit, K. R. Miller and M. D. Soucek, *Prog. Org. Coat.*, 2012, **73**, 425–434.
- 34 Y. Yoo and J. P. Youngblood, *ACS Appl. Mater. Interfaces*, 2017, **9**, 24936–24946.
- 35 Z. He, D. C. Chapital, H. N. Cheng, K. T. Klasson, O. M. Olanya and J. Uknalis, *Ind. Crops Prod.*, 2014, **61**, 398–402.
- 36 M. Samadzadeh, S. H. Boura, M. Peikari, A. Ashrafi and M. Kasiriha, *Prog. Org. Coat.*, 2011, **70**, 383–387.
- 37 H. Zhao, Q. Sun, J. Zhou, X. Deng and J. Cui, *Adv. Mater.*, 2020, **32**, 2000870.
- 38 N. H. Ramli Sulong, S. A. S. Mustapa and M. K. Abdul Rashid, *J. Appl. Polym. Sci.*, 2019, **136**, 47529.
- 39 J. Mandal, Y. Fu, A. C. Overvig, M. Jia, K. Sun, N. N. Shi, H. Zhou, X. Xiao, N. Yu and Y. Yang, *Science*, 2018, **362**, 315–319.
- 40 X. Wang, X. Liu, Z. Li, H. Zhang, Z. Yang, H. Zhou and T. Fan, *Adv. Funct. Mater.*, 2020, **30**, 1907562.
- 41 J.-F. Hoffmann, J.-F. Henry, G. Vaitilingom, R. Olivès, M. Chirtoc, D. Caron and X. Py, *Int. J. Therm. Sci.*, 2016, **107**, 105–110.
- 42 B. C. Smith, *Fundamentals of Fourier Transform Infrared Spectroscopy*, CRC press, 2011.
- 43 X. Zhang, J. Qiu, J. Zhao, X. Li and L. Liu, *J. Quant. Spectrosc. Radiat. Transfer*, 2020, **252**, 107063.
- 44 B. Zhao, M. Hu, X. Ao, N. Chen and G. Pei, *Appl. Energy*, 2019, **236**, 489–513.